Translational Stroke Research (2019) 10:216–230
https://doi.org/10.1007/s12975-018-0632-0

METHODS PAPER

A Novel Technique for Visualizing and Analyzing the Cerebral Vasculature in Rodents

Arjang Salehi[1,2] · Amandine Jullienne[2] · Kara M. Wendel[3] · Mary Hamer[2,4] · Jiping Tang[5] · John H. Zhang[5,6,7] · William J. Pearce[5,8] · Richard A. DeFazio[9] · Zinaida S. Vexler[10] · Andre Obenaus[1,2,3,4]

Received: 25 January 2018 / Revised: 27 March 2018 / Accepted: 25 April 2018 / Published online: 15 May 2018

Abstract

We introduce a novel protocol to stain, visualize, and analyze blood vessels from the rat and mouse cerebrum. This technique utilizes the fluorescent dye, DiI, to label the lumen of the vasculature followed by perfusion fixation. Following brain extraction, the labeled vasculature is then imaged using wide-field fluorescence microscopy for axial and coronal images and can be followed by regional confocal microscopy. Axial and coronal images can be analyzed using classical angiographic methods for vessel density, length, and other features. We also have developed a novel fractal analysis to assess vascular complexity. Our protocol has been optimized for adult rat, adult mouse, and neonatal mouse studies. The protocol is efficient, can be rapidly completed, stains cerebral vessels with a bright fluorescence, and provides valuable quantitative data. This method has a broad range of applications, and we demonstrate its use to study the vasculature in assorted models of acquired brain injury.

Keywords Analysis · Rodents · Vasculature · Traumatic brain injury · Stroke

Introduction

The brain is one of the most metabolically active organs in the body. In order to satisfy its high metabolic needs, the brain requires an intricate network of blood vessels that constitutes the cerebral vasculature. Cerebral vessels are responsible for maintaining constant blood flow throughout the brain [1]. Perturbations or cessation in blood flow, for example during ischemic stroke, can lead to irreparable neuronal injury in a matter of minutes [2, 3]. At the cellular level, the cerebral vessels engage with neuronal and non-neuronal cells to regulate blood flow in accordance with neuronal activity (neurovascular coupling) [1, 4, 5]. The vascular endothelium forms a restricted barrier called the blood-brain barrier, which controls the entry of molecules into the brain and is essential for creating a protective environment for neurons [1]. Thus, maintaining an intact

Electronic supplementary material The online version of this article (https://doi.org/10.1007/s12975-018-0632-0) contains supplementary material, which is available to authorized users.

✉ Andre Obenaus
obenausa@uci.edu

[1] Cell, Molecular and Developmental Biology Program, University of California, Riverside, 1140 Bachelor Hall, Riverside, CA 92521, USA

[2] Department of Basic Sciences, Loma Linda University, Loma Linda, CA 92354, USA

[3] Department of Anatomy and Neurobiology, University of California, Irvine, Irvine, CA 92697-4475, USA

[4] Department of Pediatrics, University of California, Irvine, Irvine, CA 92697-4475, USA

[5] Department of Physiology and Pharmacology, Loma Linda University School of Medicine, Loma Linda, CA 92350, USA

[6] Department of Anesthesiology, Loma Linda University School of Medicine, Loma Linda, CA 92350, USA

[7] Department of Neurosurgery, Loma Linda University School of Medicine, Loma Linda, CA 92350, USA

[8] Center for Perinatal Biology, Loma Linda University, Loma Linda, CA 92350, USA

[9] Molecular and Integrative Physiology, University of Michigan, Ann Arbor, MI 48101, USA

[10] Department of Neurology, University of California, San Francisco, San Francisco, CA 94158, USA

blood-brain barrier with blood flow regulated in response to metabolic need is crucial for cerebral health.

An important challenge facing preclinical research is to find methods to rapidly visualize the cerebral vasculature at the whole brain level. The ability to image cerebral vessels would be invaluable in understanding the vascular anatomy in healthy developing and mature brains. Neuroscientists need a reliable method to study cellular and morphological aspects of vascular pathology following a variety of brain injuries and diseases. In addition, the effects of promising therapeutics targeting the cerebrovasculature require methods for assessment. Thus, there is an urgent need to develop sensitive and more efficient techniques to visualize the cerebral vessels in the entire brain.

Several techniques have been developed that permit for visualization of cerebral vasculature of the rodent brain. One such technique is called vessel painting (VP), which was originally developed to visualize the 3D blood vessel network in the retina and was recently modified to stain the cerebral vasculature [6–8]. The VP technique utilizes a lipophilic carbocyanine dye, 1,1′-dioctadecyl-3,3,3′,3′-tetramethylindocarbocyanine perchlorate (DiI), to label endothelial cell membranes. VP is achieved through measured intracardiac injection of an aqueous DiI solution followed by perfusion fixation. When the DiI molecules come in contact with the vessel lumen, it is incorporated within the lipid membranes thereby staining the entire vessel lumen [6, 9]. Originally, a major drawback of this technique was that it had low success rate and labeled vessels typically exhibited heterogeneous staining, precluding repeatable quantitative whole or regional analysis. Furthermore, the original retinal studies were not adapted to stain the cerebral vasculature in rats.

Vascular analysis has been accomplished using manual analytical programs (ImageJ plugins) and semi- and full-automated software programs [10, 11]. A recently developed tool is AngioTool, a fully automated program that performs a comprehensive quantitative analysis focusing particularly on vessel network features and computes various morphometric and spatial parameters including number of vessels, vessel length, branching, and lacunarity, among others. AngioTool has been utilized in simple vascular systems such as murine embryonic hindbrain, retinal, and allantois explants [12]. AngioTool features have not been optimized for large-scale analysis of the rodent cerebrovasculature.

The use of fractals as a measure of complexity has not been routinely employed in neuroscience, and few reports exist for its utilization in morphological characterization of cerebral vessels [13, 14]. Fractal analyses have been used to evaluate roughness and patterning of neuron structures and microglial morphology [15–17]. Fractals have recently been used to study tumor and retinal vessels [18, 19], and we have been one of the first to use it in evaluation of whole brain rodent cerebrovasculature [20].

Here, we present a novel protocol to stain, visualize, and analyze the blood vessels in the rodent brain. Our novel VP technique has been adapted for the adult rat brain and further improved to label vessels in the adult and neonatal mouse brain. Unlike previous techniques, our technique stains cerebral vessels with a bright red fluorescence that allows for visualization by wide-field fluorescence and confocal microscopy. Another key advantage of our technique is that it stains the blood vessels in the entire brain (in 3D) across rodent species and ages. We introduce two complimentary analysis approaches that have been adapted for brain vasculature in rodents: classical analysis to assess vessel characteristics and fractal analysis to measure vascular complexity. We applied our protocol to analyze the cerebral vasculature in adult and neonatal mice and obtained quantitative parameters of vessel density, length, and complexity. Finally, we demonstrate its ability to be used in a variety of acquired brain injury models where vascular alterations are known to occur. Further, the protocol is uncomplicated, involves a minimum number of steps, and requires only a handful of standard laboratory materials.

Materials

Reagents

The following reagents were used:

- DiI (Life Technologies, Carlsbad, CA; catalog number D282)
- Ethanol (absolute, 200 proof; Fisher Scientific, Fair Lawn, NJ; catalog number BP2818100)
- Sodium nitroprusside (SNP, dihydrate, Sigma Aldrich, Saint Louis, MO; catalog umber 71778)
- Heparin, sodium injection 1000 USP units/mL (Sagent Pharmaceuticals, Schaumburg, IL; catalog number 25021-400-01)
- Phosphate buffered saline (PBS, 1×; MP Biomedicals, Solon, OH; catalog number 0928103)
- PBS contains 2.68 mM potassium chloride, 1.47 mM potassium phosphate monobasic, 136.89 mM sodium chloride, and 8.10 mM sodium phosphate dibasic at pH 7.4
- Paraformaldehyde (PFA, 32%; Electron Microscopy Sciences, Hatfield, PA; catalog number 15714-S)
- Dextrose (anhydrous, Fisher Scientific, Fair Lawn, NJ; catalog number 50-99-7)

Preparation of Reagents

DiI stock solution: 100 mg DiI, 33.4 mL 100% ethanol. Protect from light and store at room temperature for up to 1 year.

Diluent solution: 2 g dextrose, 1 mL 10× PBS, adjust with ddH_2O to 50 mL. Filter through a 0.22-μm bottle-top filter. Store at 4 °C; stable for several months. Diluent solution is warmed to 37 °C prior to adding the DiI stock solution.

DiI working solution (see Note 1):

Method 1

i. Adult rat (250 g): 200 μL DiI stock solution, 900 μL 100% ethanol, adjust with diluent solution to 50 mL.
ii. Adult mouse (25 g): 40 μL DiI stock solution, 180 μL 100% ethanol, adjust with diluent solution to 10 mL.

Method 2

i. Adult mouse (25 g): 50 μL DiI stock solution, 450 μL diluent solution.
ii. Neonatal mouse (12 g): 25 μL DiI stock, 225 μL of diluent solution.

SNP stock solution: 0.75 mg SNP, 1 mL sterile 1× PBS. Protect from light and refrigerate at 4 °C. Stable for 1 week.

SNP-heparin injection solution: 0.75 mg/kg SNP stock solution, 2000 units/kg heparin (see Note 2).

Equipment

Method 1
Nitrogen tank
Two 100-mL bottles
PE-50 tubing
Tygon lab silicone tubing, 1/32 in. (Cole-Parmer, Vernon Hills, IL)
Three-way stopcock (cat# WU-30600-02, Cole-Parmer)
22-Gauge Luer stub adapters (cat# 724439, Harvard Apparatus, Holliston, MA)
Male to male Luer lock connectors (cat# 12090, Qosina, Edgewood, NY)
Pressurized air tank, 2 L empty plastic bottle with airtight cap
27-Gauge Luer stub
30-Gauge needle
1-mL syringe with barrel flange cut
10-mL syringe
Syringe pump (Harvard Pump II Plus single syringe, Harvard Apparatus, Holliston, MA)

Method 2
Two 100-mL bottles
FH100 peristaltic pump (Thermo Fisher Scientific, Waltham, MA)
1-mL syringe with 23-gauge needle
1-mL syringe with barrel flange cut
Tygon lab silicone tubing, 1/32 in.

Methods

Two Methods to Stain the Cerebral Vasculature

Method 1 Procedure

Method 1 was initially based on a protocol developed for mice by Hughes and colleagues [6], and modifications to the protocol were made to improve the efficiency and facilitate its use in rats (Fig. 1a). The initial protocol utilized a pressurized air tank with a blood pressure bulb and gauge to deliver the perfusion solutions, but air leakage often resulted in an inability to maintain constant pressure throughout the system. Thus, to overcome these limitations, we switched to a nitrogen gas tank that provided continuous delivery of perfusion solutions under careful and constant pressure (1.7 PSI). PBS and PFA solutions were then delivered under constant pressure, while the DiI solution was delivered under constant flow rate using a syringe pump. The three-way stopcock assembly was used to control the solutions flowing from the outflow port (Supplemental Fig. 1).

1. Assemble the perfusion apparatus. A detailed description of how to construct the perfusion apparatus can be found in Hughes' article [6] (Supplemental Fig. 1). As stated above, the blood pressure bulb and gauge was replaced with a nitrogen gas tank.
2. Before starting the procedure, it is imperative that the entire system is airtight and devoid of air bubbles.
3. Anesthetize mouse or rat by intraperitoneal injection of ketamine (90 mg/kg) and xylazine (10 mg/kg) or by other institutionally approved method.
4. In a perfusion tray, secure the animal on its back. Make an incision along the thoracic midline to open the abdominal cavity. Cut the diaphragm. Carefully cut the chest wall on both sides. Take a small hemostat to hold the sternum and turn it toward the head to expose the chest cavity.
5. Inject the SNP-heparin solution (0.75 mg/kg SNP stock solution and 2000 units/kg heparin) into the left ventricle.
6. Insert the butterfly needle from the perfusion device into the left ventricle and then make a large incision in the right atrium.
7. Rotate the stopcock knob for the PBS to the "on" position. Perfuse with 1× PBS (rats 150 mL, mice 10 mL) to remove the blood. A sign of a good perfusion is uninterrupted flow of blood exiting the right atrium.
8. Rotate the stopcock knob for the DiI solution to the "on" position and then activate the syringe pump. Perfuse with DiI solution (rats 50 mL, mice 10 mL) at a constant flow rate (rats 10 mL/min, mice 1 mL/min). During perfusion with DiI solution, the nose and palms of the animal will turn slightly pink.

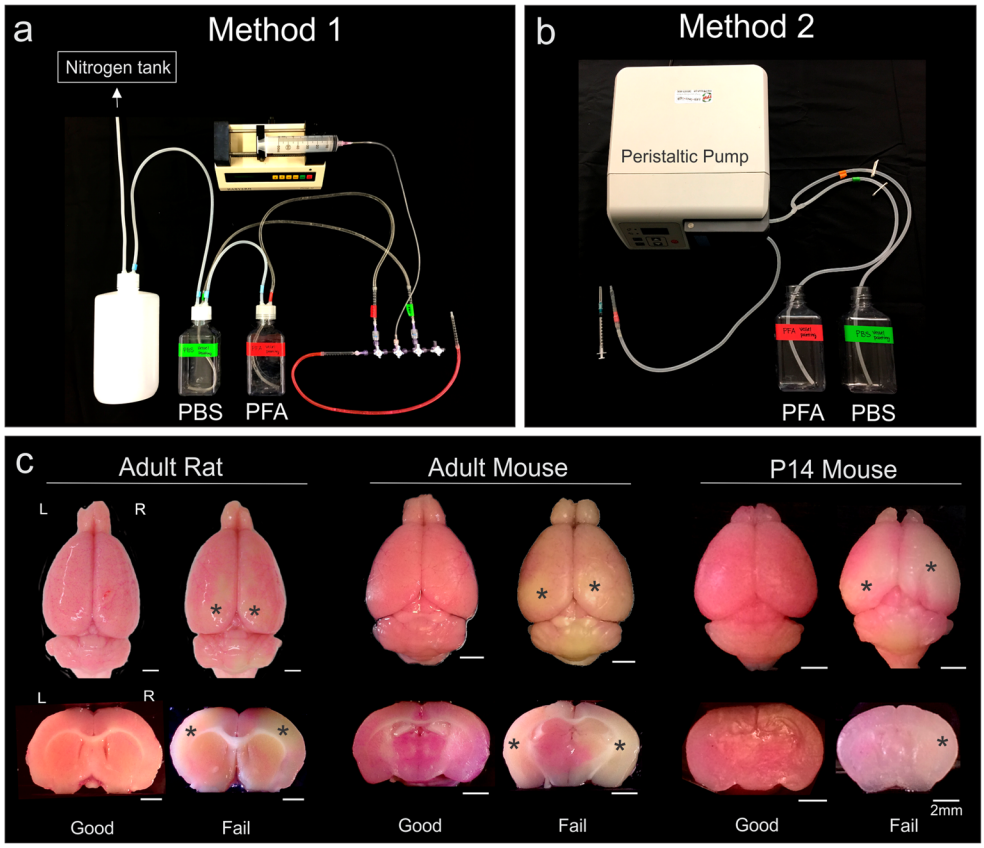

Fig. 1 Vessel painting perfusion apparatus for rodents. **a** Photograph of vessel painting (VP) apparatus for adult mice and rats (Method 1) used in our studies. The apparatus consists of a nitrogen tank, tubes connecting to the stopcock assembly, and an outflow port. The nitrogen tank provides pressure to deliver the phosphate buffered saline (PBS) and paraformaldehyde (PFA) fixative solutions. **b** Photograph of VP apparatus for adult and neonatal mice (Method 2). This setup consists of a peristaltic pump and syringe containing the DiI solution. The pump is used to deliver the PBS and PFA, but the DiI solution is delivered manually. **c** Representative examples of VP in adult mice and rat brains as well as in postnatal day 14 (P14) mouse brain. The brains labeled "good" demonstrate successful VP with uniform pink staining of the tissue. The brains labeled "fail" demonstrate failed VP perfusion with patches of pale tissue (asterisks) within the diffusively pink tissue. Right hemisphere (R) and left hemisphere (L). Scale bar = 2 mm

9. Rotate the stopcock knob for the PFA to the "on" position. Perfuse with 4% PFA (rats 200 mL, mice 20 mL) to fix the brain tissue.
10. Remove brain from the skull and postfix in 4% PFA for 24 h. Brains can be left in 1× PBS in the dark for several weeks at 4 °C.

Method 2 Procedure

While method 1 works in adult mice, visual examination found that a majority of mice (75%) showed heterogeneous staining of the cerebral vessels. Imaging of vessel-painted brains revealed lack or reduced staining of capillary structures indicating that the DiI solution was not successfully penetrating into the capillaries using nitrogen tank as the pressure source. To improve circulation of the DiI solution into these fine vessels in the mouse brain, we modified the method 1 protocol by direct manual injection of the DiI solution into the left ventricle of the heart (Fig. 1b). By performing an intracardiac injection of DiI solution into a beating heart prior to the PBS perfusion step, this allows for the DiI to circulate through the entire cerebral vasculature, thereby labeling all the blood vessels, including fine capillaries. The PBS and PFA solutions were then delivered at a pulsating flow rate using a peristaltic pump (9 mL/min for adult mice and 5 mL/min for neonatal mice). The labeling efficiency rate for the adult and neonatal mice was higher with the peristaltic pump than the compressed gas nitrogen tank as the pulsating flow rate perfusion possibly better mimics the physiological conditions in the mouse than the constant pressure perfusion. The syringe pump, stopcock assembly, and its associated components are not needed for method 2 (see Note 3 for methodological differences between methods 1 and 2).

1. Before starting the procedure, make sure that the perfusion line is devoid of air bubbles.

2. Anesthetize mouse or rat by intraperitoneal injection of ketamine (90 mg/kg) and xylazine (10 mg/kg) or by other institutionally approved method.
3. Secure the animal on its back and open the abdominal cavity. See step 4 in method 1 for more detail.
4. Inject the SNP-heparin solution (0.75 mg/kg SNP stock solution and 2000 units/kg heparin) into the left ventricle.
5. Manually inject the DiI solution (adult mice 500 μL, neonatal mice 250 μL) into the left ventricle slowly over the course of 10–12 s (see Note 4). In a few cases, the heart in neonatal mice stopped beating as the DiI solution was being injected, and the heart was manually pumped using forceps to assist in circulating the solution (see Note 5). During incubation with the DiI solution, the nose and palms of the animal will turn slightly pink.
6. Insert the butterfly needle from the perfusion device into the left ventricle and then make a small incision in the right atrium.
7. Perfuse with 1× PBS (adult mice 10 mL, neonatal mice 8 mL) to remove the blood. A sign of a good perfusion is uninterrupted flow of blood exiting the right atrium.
8. Perfuse with 4% PFA (adult mice 20 mL, neonatal mice 15 mL) to fix the brain tissue.
9. Remove brain from the skull and postfix in 4% PFA for 24 h. Brains can be left in 1× PBS in the dark for several weeks at 4 °C.

Different variations of our VP protocol have been utilized in other studies and are described in Note 6.

Removal of Brain and Assessment of Vessel Painting Success

To assess the success of our VP, brains were carefully removed from the cranium without damaging the vasculature or the underlying tissues. The dura mater was gently removed from the surface of the brain keeping the pial vessels intact within the pial and arachnoid layers. Extracted brains were then postfixed in 4% PFA for 24 h before being placed in 1× PBS. Success of VP was confirmed by visual inspection of the brain parenchyma. Excellent VP was determined if brains had uniform pink staining of the surface and deep structures of the brain (Fig. 1c) and excellent labeling of pial, penetrating, and parenchymal vessels assessed by wide-field fluorescence microscopy (Fig. 2). Animals that did not meet these criteria were excluded from subsequent analysis. Method 1 showed excellent vessel staining from 67% (6/9) of adult rats and 25% (6/24) of adult mice; method 2 showed excellent vessel staining from 71% (5/7) of adult mice and 37.5% (6/16) of neonatal mice (Table 1). Failed vessel-painted brains exhibited heterogeneous staining and pale spots within the pink tissue (Fig. 1c, asterisks). Vessel-painted brains with lack of pink staining were classified as "no staining." Methods 1 and 2 have also been utilized in other applications and their success rates are reported in Note 7.

Wide-Field Fluorescence Imaging of Vessel-Painted Brains

Vessel-painted brains were imaged by wide-field fluorescence microscopy (BZ-X700, Keyence Corp, Osaka, Japan). The BZ-X700 fluorescent microscope can image to a depth of 42 μm which allows for imaging of the surface cortical vessels and parenchymal vessels of the brain. Acquisition of whole brain axial images of the dorsal view was executed through careful positioning of the brain between two glass slides. Gentle pressure was applied to minimally flatten the dorsal surface of the brain to facilitate imaging of the entirety of the surface cortical vascular network of the cerebrum without causing damage (Supplemental Fig. 2). The brains were gently pressed onto the glass slides until the compression ring is formed in the outer perimeter of the brain resulting in clear view of the middle cerebral artery trunk and its branching vessels. Z-stacks of the surface cortical vessels were obtained at 2x magnification at 1-mm depth of field to collect VP data as the cortical surface curves laterally. Following acquisition, axial Z-stacks were merged into full focus images using BZ-X Analyzer software (Keyence Corp, Osaka, Japan). After axial images were collected, coronal images were obtained by placing brains into an Acrylic Brain Matrix (Ted Pella, Inc., Redding, CA) and slicing 5 mm posteriorly from the olfactory bulbs to create an anterior and posterior half brain. The posterior half brain was placed on a glass slide (Supplemental Fig. 2) and imaged at ×2 magnification at 1-mm depth of field. The coronal Z-stacks were merged into a full focus images.

Axial view images revealed uniform staining of the cortical vessels on the surface of the brain (Fig. 2, top row). The pial vessel network, including branching arteries from the middle, anterior, and posterior cerebral arteries and leptomeningeal anastomosis, is clearly visible in our axial images. However, there was limited staining of the superior sagittal sinus, transverse sinuses, and other venous structures (see Note 8 for limitations of our VP protocol). Coronal images of the anterior half brains confirmed well-defined staining of deep vessel structures within the brain (Fig. 2, bottom row). We observed distinct labeling of the penetrating vessels on the cortical surface and parenchymal microvessels in subcortical brain regions. Furthermore, there was no apparent leakage of the DiI working solution from the vessels into the cerebral tissue.

High-Resolution Confocal Microscopy

The DiI molecule has an intense fluorescence and fades slowly when exposed to excitation light during image acquisition [21]. Given its strong fluorescence intensity and slow fading properties, we tested whether DiI-labeled vessels are

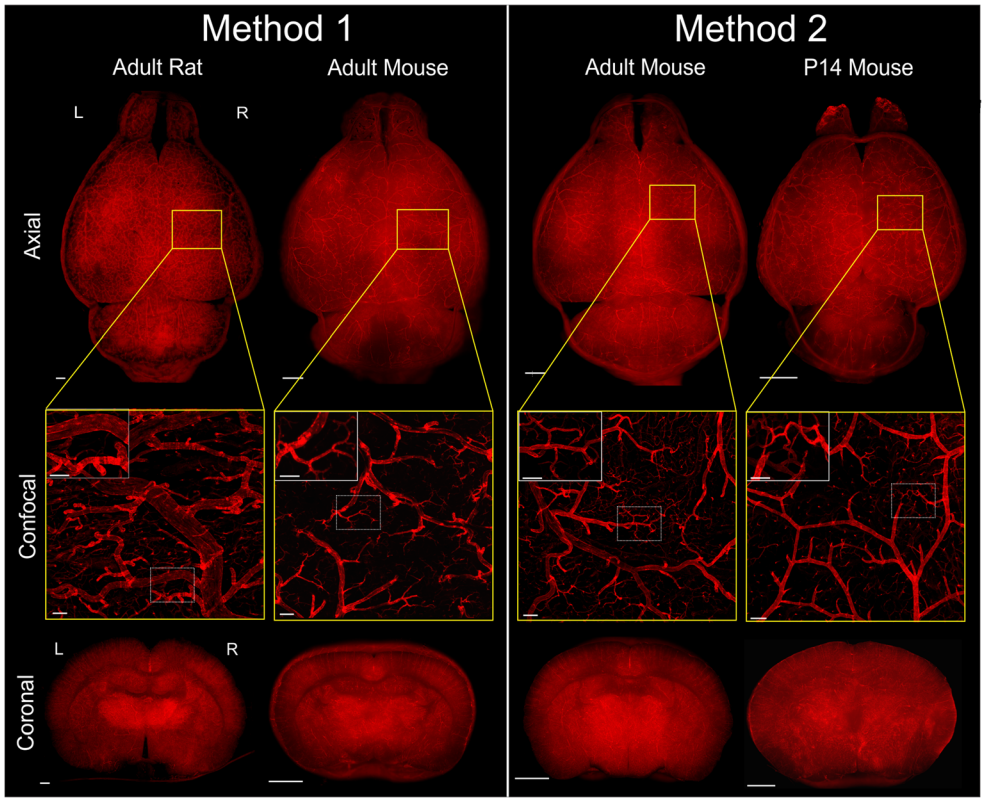

Fig. 2 Visualization of a mouse and rat brains. The top row displays examples of axial view images of adult rat and mouse brains as well as P14 mouse brain. The middle row set of images are high-magnification confocal images from axial cortical tissues, and the bottom row shows coronal images. The representative brains from either method 1 or 2 illustrate excellent staining of all the blood vessels within whole brain tissues. The confocal images confirm crisp staining of pial, penetrating, and parenchymal microvessels. Adult mouse brain stained with method 2 revealed more uniform staining of large pial vessels and intense staining of microvessels than method 1 (see confocal images). The boxed areas in the confocal images are magnified in the inserts. Right hemisphere (R) and left hemisphere (L). Scale bar = 1 mm (axial and coronal images), 200 μm (confocal), and 100 μm (inserts). Axial and coronal VP brain tissue were scaled to the same size for rats and mice

amendable to laser scanning confocal microscopy. Laser scanning confocal microscopy (Zeiss LSM 710 NLO, Jena, Germany) was used to acquire axial images from the dorsal surface of the cortex (wavelength absorbance 549 nm, emission 565 nm). Axial views of the brain were obtained between the middle and anterior cerebral arteries using a ×5 magnification with 300-μm depth of field. Images were subsequently processed to create maximum intensity projections using Zeiss software (Zeiss Zen 2010, Jena, Germany).

Axial confocal images revealed uniform staining of the pial, penetrating, and microvessels on the surface of the brain (Fig. 2, middle row). Adult mice stained with method 1

Table 1 Evaluation of vessel-painted brains following methods 1 and 2

Method	Excellent[a]	Failed[b]	No staining[c]	Success rate[d] (%)
Method 1—adult rat	6	3	0	67
Method 1—adult mouse	6	5	13	25
Method 2—adult mouse	5	2	0	71
Method 2—P14 mouse	6	5	5	37.5

The table summarizes the number of vessel-painted brains with excellent, failed, and no staining following methods 1 and 2

[a] Excellent vessel-painted brains exhibited homogeneous pink staining of the entire brain parenchyma and excellent labeling of vessels on the dorsal surface and deep compartments in the brain - see Fig 1c

[b] Failed vessel-painted brains exhibited heterogeneous pink staining and poor labeling of vessels in the brain

[c] Brains with lack of pink staining were classified as "no staining"

[d] The success rate was determined by dividing the number of excellent vessel-painted brains by the total number of brains

typically showed heterogeneous staining of large vessels and reduced or absent staining of microvessels, while adult mice stained with method 2 had more uniform staining of large vessels and improved microvessel staining (compare confocal images of adult mice from method 1 and method 2). We detected small red aggregates attached to the vessel lumen using method 1, which have been reported in other VP protocols [22, 23]. These dye aggregates were absent from adult mice stained with method 2.

Classical Vascular Analysis

Wide-field fluorescence and/or confocal images can be utilized in a broad range of analysis methods. Quantitative analysis of vessel characteristics has previously been reported for simple vascular systems such as retinal explants (AngioTool) [12]. For the first time, we demonstrate that AngioTool can be utilized for large-scale vascular analysis of the rodent brain (Fig. 3b, c). Analysis of the cerebrovasculature can be undertaken from the entire cortical surface or in regional sections based on the scientific question being studied. Herein, we describe our analysis of the blood vessels from the left and right hemispheres.

Using BZ-X Analyzer software, the raw fluorescent images were first processed for black balance and haze reduction (blur/brightness/reduction 10/10/1) to enhance the appearance of the vessels from wide-field fluorescent images (Fig. 3a). The processed fluorescent images displayed high resolution of the labeled vessels with reduced background signal (Supplemental Fig. 3). The processed images were then imported into Fiji ImageJ software (http://fiji.sc/) and regions of interest (ROIs) were drawn around the left and right hemispheres. The compression ring around the edge of the brain was excluded from the analysis by drawing a ROI that encompassed the brain surface along the curvature of the brain. The ROIs were saved and imported to AngioTool software. The software then selects vessels based on their diameter and fluorescence intensity and the values can be individually adjusted. For whole brain analysis, the vessel diameter was set to 2 which selects vessels with diameters greater than 2 μm. The vessel intensity was set from 0 (minimum) to 255 (maximum) which indicates that vessels with a large range of fluorescence intensity (faint to bright) were included in the analysis. The classical vascular analysis generates an AngioTool image related to the number of vessels and their branch points (Fig. 3b). The size and color of the features can be user adjusted, where the AngioTool image displays vessels in red, branch points in blue, and vessel area outlines in yellow. Additionally, the software provides vessel morphometric and spatial features, including vessel area, total number of junctions, number of endpoints, and total vessel length (Fig. 3c, see Note 9 for limitations of classical analysis). A detailed description of these parameters can be found in the article from Zudaire and colleagues [12].

Fractal Geometry Analysis

The complex vasculature of the rodent brain can also be quantified by fractal geometric analysis [13]. The use of fractals to analyze vascular structures is rare, and in the few reported studies, it is used to assess retinal or tumor vessels [18, 19]. We have developed a novel fractal analysis protocol that has been adapted for analyzing the rodent cerebrovasculature (Fig. 3d–f). Our fractal analysis provides unique and complimentary data on vascular complexity of the whole brain, which cannot be derived using the classical vascular analysis method (see Note 10 for differences between classical and fractal analysis).

Processed axial images were imported into Fiji software and converted into a binary image. The polygon tool was used to outline the ROIs on the whole brain hemispheres. Fractal analysis was performed using the ImageJ plugin that was developed for microglia analyses, FracLac [24]. A local fractal dimensions (LFD) analysis was performed from the binary images at each pixel using the box counting method. The method applies the following formula $D_{\mathrm{Bmass}} = \lim_{\varepsilon \to 0} [\ln(\mu_\varepsilon)/\ln(\varepsilon)]$, where ε is the side length of the box and μ_ε is the mean pixels per box of side ε. A $\ln(\mu_\varepsilon)$ vs. $\ln(\varepsilon)$ graph is generated and LFD is calculated by taking the slope of the log regression line [15]. All output data and graphs were saved. Following analysis, the software generated a colorized image visually encoding the degree of complexity (Fig. 3d) where the color scale used can be adjusted by the user (lookup table LUT4 used in this study) (Fig. 3e). The brain vasculature is colorized with a gradient of low LFD (low complexity) in blue, medium LFD (medium complexity) in yellow, and high LFD (high complexity) in pink. The different colors correlate with the complexity of vessels, with large pial vessels appearing more complex than microvessels. The distribution of LFD displays a histogram with local fractal dimensions (complexity) in the *x*-axis and frequency (vessel number) in the *y*-axis (Fig. 3f). Kurtosis, skewness, and peak fractal frequency values are extracted from the fractal histograms. Kurtosis describes the peakness (tailness) of the fractal distribution, skewness describes the uniformity of the fractal distribution, and peak fractal frequency is the peak fractal value.

Notes

1. Direct labeling of the cerebral vessels was achieved through the lipophilic carbocyanine dye DiI ($DiIC_{18}$ (3)), a lipid-soluble molecule that becomes incorporated into endothelial cell membranes upon contact. To facilitate efficient circulation of the DiI in the rodent

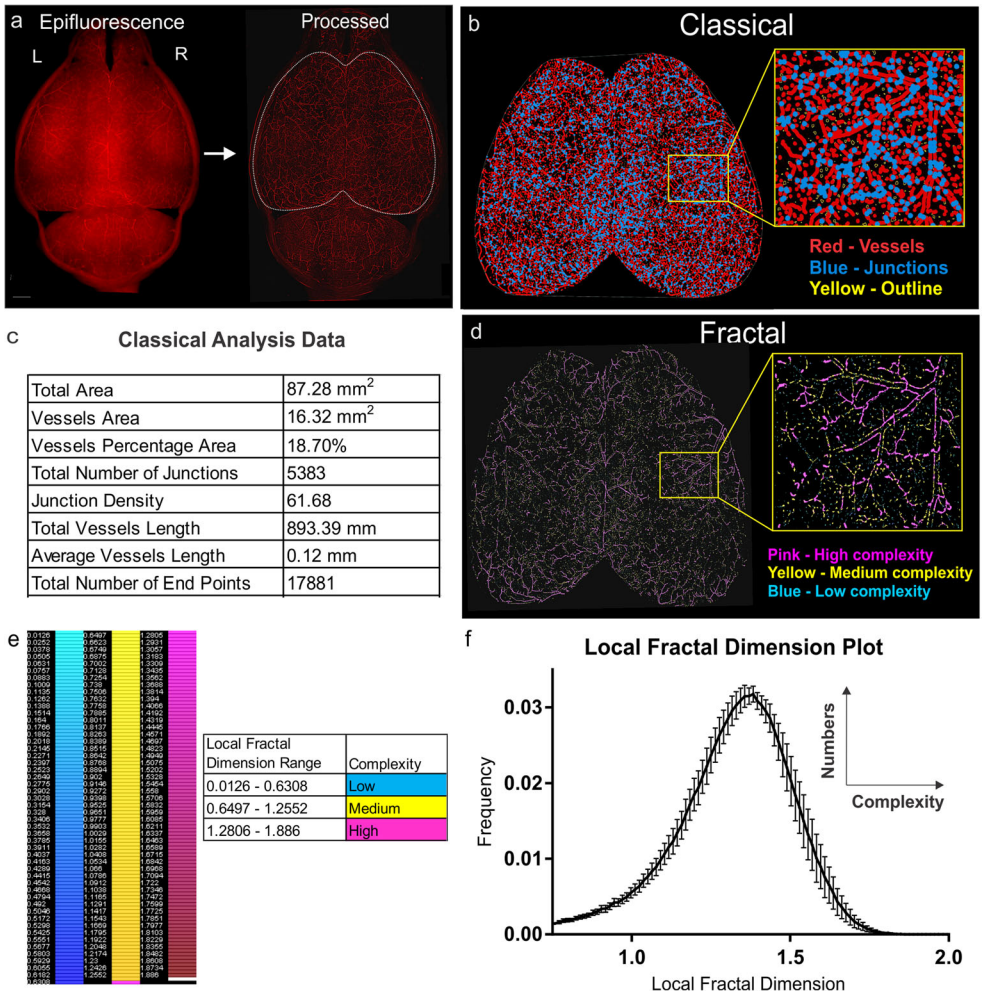

Fig. 3 Classical and fractal vascular analysis of vessel-painted images. **a** The raw epifluorescent image is processed using black balance and haze reduction algorithms to create an enhanced fluorescent image with reduced background. A region of interest is drawn around the whole cortex (white outline). Right hemisphere (R) and left hemisphere (L). **b** The enhanced image can be processed for vascular features (AngioTool software) which results in images that display vessels in red, junctions in blue, and vessel outline in yellow. **c** Quantitative analysis of vessel characteristics can be derived including vessel percentage area, number of junctions, vessel length, and lacunarity. The data is from the enhanced fluorescent image from Fig. 1a. **d** The enhanced image can be processed for vascular complexity using fractal analysis (FracLac, ImageJ plugin). The fractal analysis extracts the local fractal dimension (LFD) and then color-codes according to the degree of vessel complexity. The vasculature in the brain is colorized based on corresponding fractal dimension with a gradient from lower LFD in blue (less complex) to higher LFD in pink (more complex). **e** The color scale displays LFD values with a gradient from blue (less complex) to pink (more complex). The LFD value ranges and vessel complexity are shown in the chart. **f** The resultant LFD histogram displays vessel complexity in the *x*-axis (LFD) and vessel numbers in the *y*-axis (frequency). The histograms can be quantitatively analyzed by measuring skewness, kurtosis, and LFD peak frequency. The histogram is a mean of 4 animals with all error bars presented as standard error of mean

circulatory system, an aqueous DiI working solution was prepared as previously described [6, 7]. This aqueous DiI working solution contains high concentrations of PBS along with dextrose in order to maintain osmolarity. In our preliminary work, we found that DiI had a tendency to precipitate out of solution at room temperature and this issue was resolved by heating the solution at 37 °C prior to injection.

2. The doses for SNP (vasodilator) and heparin (anticoagulant) were based on previously published work [6]. The SNP-heparin injection prevents blood clot formation, improves homogeneity of the staining, and enhances DiI solution penetration into microvessels, facilitating improved vessel resolution.
3. There are several differences in methodology that must be noted. First, method 2 is reliant on intrinsic blood flow to circulate the DiI solution throughout the brain. As a result, this procedure only labels blood vessels with active perfusion. In cases when cerebral blood flow is reduced or absent, such as in acquired and nonacquired brain injuries, this could potentially affect the quality of the vessel staining and lead to poorly labeled vessels. Conversely, method 1 is reliant on the PBS solution (under constant pressure) to remove the blood throughout

the cerebrovasculature and subsequent delivery of DiI solution to label the vessels. Method 1 does not rely on the heart to circulate the DiI solution. Second, each method used different concentrations of the DiI working solution (12.8 μM for method 1 vs. 321 μM for method 2). The total volumes were also adjusted according to the rodent strain and age. We found that these DiI concentrations effectively labeled all the blood vessels in the entire mouse and rat brain, while also preventing the formation of dye aggregates. Third, the order in which the perfusion solutions were delivered differs between methods. Method 1 delivered the DiI solution following the PBS solution, while method 2 delivered the DiI solution prior to the PBS solution.

4. It is imperative that DiI working solution is injected at a steady rate. Following injection, quickly start the perfusion with PBS and PFA solutions. A long delay at this step can lead to incomplete vessel painting.
5. The VP procedure in neonates was challenging because of their small size and difficulty in performing injections and insertion of the butterfly needle into the heart. Some neonates underwent cardiac arrest during the intracardiac injection inhibiting the circulatory system from naturally distributing the DiI solution throughout the brain. If cardiac arrest did occur, the heart was manually pumped to create perfusion but in a limited capacity. A possible modification could be to inject a smaller volume of DiI solution and administer it at a slower pace. Additionally, the SNP-heparin injection could be administered several minutes prior to VP procedure.
6. A very recent modified VP protocol has been shown to label blood vessels in adult and neonatal mice [23, 25]. This modified technique resembles our method 1 procedure but with a few minor modifications: SNP-heparin was injected subcutaneously 5 min prior to euthanizing, and infusion of PBS and PFA solution was performed with a peristaltic perfusion pump. The authors reported strong labeling of pial vessel network on axial images, but it was unclear whether this modified protocol stained parenchymal vessels as efficiently as our technique. A recent study by Konno and colleagues [22] utilized neutral liposomes and $DiIC_{12}$ to achieve brighter and uniform labeling of the blood vessels in the mouse brain. The addition of liposomes to the DiI solution prevented the formation of DiI aggregates which improved the homogeneity of the vessel painting. This technique is similar to our method 1 procedure, except that the PBS flush was omitted and DiI/liposome solution was manually injected.
7. Method 2 has been utilized in healthy female mice with a success rate of 67% [26]. We previously utilized method 1 in adult rats that received moderate TBI and found that 70% of rat brains showed excellent vessel staining [20]. Similarly, we used method 2 in adult male mice that received a moderate TBI and found that 65% of mouse brains showed excellent vessel staining including labeling of new, immature microvessels [9].
8. The VP protocol described here has several limitations. First, DiI may label cerebral arteries and veins differently, a feature that is difficult to elucidate. Other protocols that use DiI reported high staining of arteries and arterioles and limited staining of veins and venules [6, 23]. Based on these studies, we do not recommend this VP protocol if one has an interest in studying the cerebral venous system. Second, this protocol provides only a snapshot of the cerebral vasculature at a single time point in an individual animal. Thus, large numbers of animals are needed to study temporal alterations of the cerebral vessels over time. Techniques for real-time imaging of the in vivo brain vasculature are available and these could be combined with our protocol [27, 28]. Third, while this protocol enables visualization of the blood vessels in the entire brain, it does not provide meaningful data on blood flow. Noninvasive techniques such as magnetic resonance perfusion-weighted imaging (PWI MRI) or two-photon approaches could be utilized prior to VP to provide dynamic information on blood flow [29, 30]. This is of particular importance in brain pathologies where blood flow is reduced or heterogeneous [31]. Since effective labeling is predicated on perfusion of DiI through the vessels, labeled vessels must possess some degree of blood flow or the capacity to perfuse blood (and likely a mature vessel lumen). Thus, this protocol offers only indirect data regarding perfusion status of the vessels.
9. One limitation of our analysis approaches is that it does not report on average vessel diameter which would be useful in determining the type of blood vessels. An alternative approach would be to measure vessel diameter with ImageJ plugins such as Vessel Diameter or Vessel Analysis.
10. The classical and fractal analyses apply different parameters and algorithms for quantification and measure distinct features of the vessel network. For the classical

Fig. 4 Workflow of vessel painting and analysis. The workflow is comprised of four components, the actual vessel painting technique (two methods), data acquisition, analysis methods, and extraction of the final results. The vessel painting technique consists of two methods: one optimized for the adult rat and mouse (method 1) and a second modification for adult and neonatal mouse (method 2). Following the procedure, vessel-painted brains are removed from the cranium, visually inspected to ensure adequate staining, and imaged by wide-field and/or high-resolution fluorescence microscopy. The raw fluorescent images are processed and subsequently analyzed by classical and fractal analysis. Classical vascular analysis provides quantitative analysis of vessel characteristics and creates an image that displays vessels and branch points. Fractal geometric analysis measures biological vessel complexity and creates a colorized image according to the degree of complexity

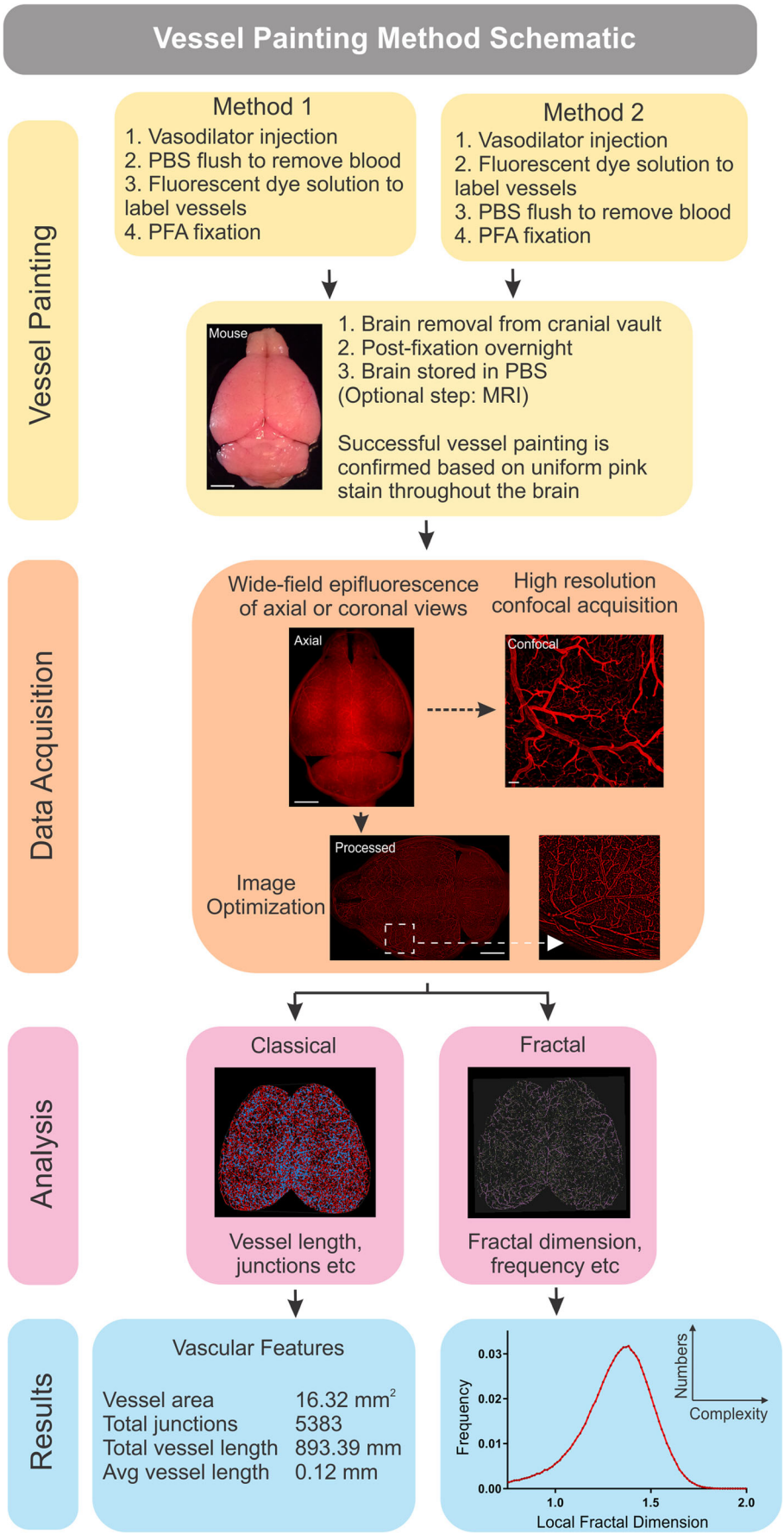
Vessel Painting Method Schematic
Vessel Painting
Method 1
1. Vasodilator injection
2. PBS flush to remove blood
3. Fluorescent dye solution to label vessels
4. PFA fixation
Method 2
1. Vasodilator injection
2. Fluorescent dye solution to label vessels
3. PBS flush to remove blood
4. PFA fixation
Mouse
1. Brain removal from cranial vault
2. Post-fixation overnight
3. Brain stored in PBS
(Optional step: MRI)
Successful vessel painting is confirmed based on uniform pink stain throughout the brain
Data Acquisition
Wide-field epifluorescence of axial or coronal views
High resolution confocal acquisition
Axial
Confocal
Processed
Image Optimization
Analysis
Classical
Fractal
Vessel length, junctions etc
Fractal dimension, frequency etc
Results
Vascular Features
Vessel area 16.32 mm²
Total junctions 5383
Total vessel length 893.39 mm
Avg vessel length 0.12 mm
Frequency
0.03
0.02
0.01
0.00
1.0
1.5
2.0
Local Fractal Dimension
Numbers
Complexity

analysis, AngioTool identifies vessel segments using a multiscale Hessian enhancement filter [32]. A vessel segment is defined as any segment between two branch points, two end points, or a branch point and an end point. Vessel segments are skeletonized and then analyzed by counting and morphometric algorithms which compute various morphological features of the vessels. For the fractal analysis, FracLac assigns fractal properties to the blood vessels in the image [15]. Fractals are defined as geometric patterns that are repeated across different scales. An LFD analysis is performed at each pixel using the box counting method to measure fractal dimensions (quantitative index of complexity) and frequency (number of occurrences in each box). The resulting fractal data measures morphological complexity in the entire vessel network.

Application of the Vessel Painting Procedure

We have synthesized the process of VP and analysis into a schematic that provides an overview (Fig. 4). Additional details are described in the text. We now discuss the applications of our VP technique and analyses.

Classical and Fractal Analysis of Cerebral Vessels in Adult and Neonatal Mice

To validate our vessel painting technique and vascular analysis approaches for particular detection of a range of blood vessel sizes in the brain, we analyzed the cortical vasculature in healthy adult (8-week-old, 25–28 g, Jackson Laboratories, $n = 4$) and neonatal (P14, 10–12 g, Jackson Laboratories, $n = 4$–5) male C57BL/6 mice. The vasculature of adult and neonatal mice were labeled with method 2, and whole brain axial images were obtained and analyzed by classical vascular analysis, as described above. Comparison of classical vascular analysis images revealed reduced vessel features in neonatal brain compared to the brain of adult mice (Fig. 5a). Vascular analysis of the entire hemispheric cortex demonstrated reductions in vessel percentage area (16.3 ± 2.1 vs. $21.3 \pm 1.1\%$, unpaired Student's t test, $p < 0.05$), total number of junctions ($7.3 \times 10^{-4} \pm 9.6 \times 10^{-5}$ vs. $1.5 \times 10^{-3} \pm 1.3 \times 10^{-4}$, unpaired Student's t test, $p < 0.05$), and total vessel length ($1.4 \times 10^{-4} \pm 9.1 \times 10^{-6}$ vs. $2.1 \times 10^{-4} \pm 1.1 \times 10^{-5}$mm, unpaired Student's t test, $p < 0.05$) in neonatal mice as compared to adult mice (Fig. 5b). There was an increase in lacunarity (space between vessels) (unpaired Student's t test, $p = 0.08$) in neonatal mice brains as compared to adult brains but this did not reach significance (Fig. 5b). Collectively, these data suggest that vessel characteristics in the cortex increase from adolescence to adulthood.

We next analyzed vascular complexity between the adult and neonatal mice vasculature using fractals. Comparison of fractal colorized images revealed a reduction in vessel complexity in neonatal brain as compared to the brain of adult mice (Fig. 5c). When we analyzed the entire hemispheric cortex, we observed a leftward shift (reduced vascular complexity) and a decrease in peak frequency values (reduced vessel numbers) in the histogram from the neonatal mice brains compared to the adult brains (Fig. 5d). Quantitative analysis of the distribution of the LFD revealed a 3.9% reduction (unpaired Student's t test, $p = 0.30$) in skewness and 22.6% reduction (unpaired Student's t test, $p = 0.11$) in kurtosis values but did not reach significance. The peak frequency value, a measure of the number of vessels, revealed a 5% reduction in neonatal mice (unpaired Student's t test, $p = 0.08$) compared to the adult mice, but this did not reach significance. While the complexity values were not significantly different between neonatal and adult brain, there was a clear increase in vascular complexity as the mice progressed to adulthood. These changes in the cerebral vasculature are consistent with other published studies [27, 33, 34].

Assessment of Vascular Architecture in Various Animal Models of Brain Injury

A critical question for our vessel-painted technique is whether it could also be used to study the vasculature following acquired brain injuries where the vasculature is known to be compromised. To test this, we induced brain injuries in adult male Sprague-Dawley rats (2–3 months old, 250–275 g, Harlan Laboratories) using a moderate controlled cortical impact (CCI) model of traumatic brain injury (TBI) [20], collagenase-induced intracerebral hemorrhage (ICH) [35], endovascular perforation-induced subarachnoid hemorrhage (SAH) [36], and permanent middle cerebral artery occlusion model (MCAO) model of ischemic stroke [37]. Injured rats underwent method 1 vessel painting at 24 h following injury. Rats with a moderate CCI showed a loss of the cortical and subcortical vessels in the right somatosensory cortex (Fig. 6a). The injury extended to a depth of about 0.5 mm confirming the moderate nature of the brain injury. ICH resulted in loss of vessels in the right striatum at the site of hemorrhage (Fig. 6c). The SAH model induced bleeding in the subarachnoid space at the base of the brain (Fig. 6c). In this model, the injury site is external to the brain parenchyma; however, there was a clear deformation of the brain tissue indicative of brain swelling. One intriguing finding in the SAH model was that there was loss of microvessels which accentuated the resolution of the pial and penetrating vessels (see axial view). This is likely due to the edematous compression of the brain. Rats with a permanent MCAO showed a clear loss of vascular components in the right hemisphere which is evident on the coronal and axial views (Fig. 6d). There was also expansion of the ipsilateral

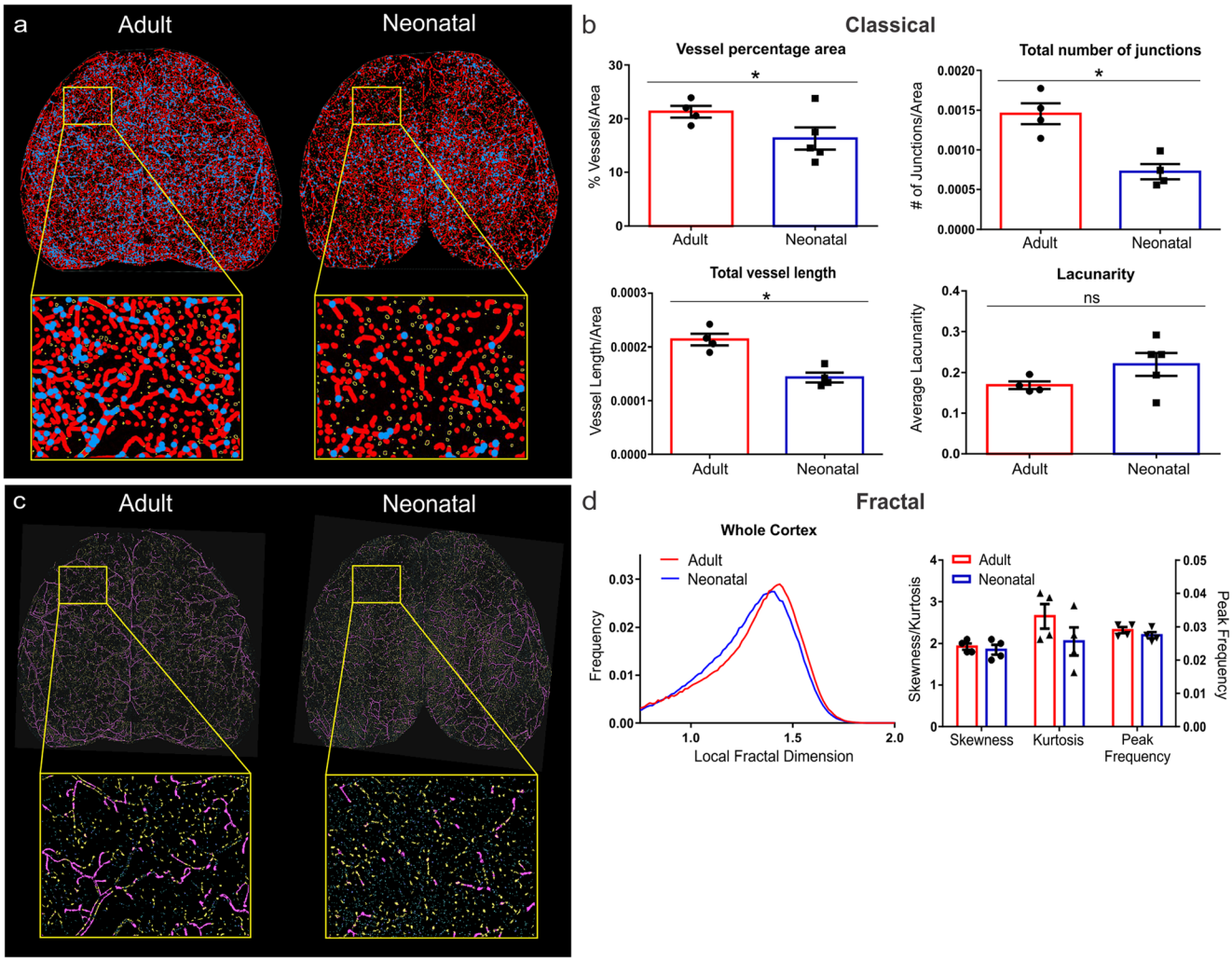

Fig. 5 Classical and fractal analysis of vessel-painted adult and neonatal mouse brains. **a** Axial images from classical vascular analysis reveal a reduction in cortical vascular features in neonatal (P14) as compared to adult (8-week-old) mice. The expanded view clearly illustrates decreased vessel density in the cortex that increases during development. Vessels (red), junctions (blue), vessel outline (yellow). **b** Whole cortex analysis demonstrates a reduction in vessel percentage area (unpaired Student's *t* test, $p < 0.05$), total number of junctions (unpaired Student's *t* test, $p < 0.05$), and total vessel length (unpaired Student's *t* test, $p < 0.05$) in neonatal mice compared to adults. There was an increase in lacunarity (unpaired Student's *t* test, $p = 0.14$) in neonatal mice as compared to adults but did not reach significance. **c** Axial images from fractal geometric analysis reveal a reduction in vessel complexity in neonatal brain (P14) as compared to adult (8-week-old) brain. The expanded view illustrates decreased complexity within the cortex. Low complexity (blue), medium complexity (yellow), and high complexity (pink). **d** Local fractal dimension (LFD) distribution in the whole cortex is representative of a decrease in vessel complexity (leftward LFD shift) and a decrease in vessel numbers (decreased peak frequency). Quantitative analysis of the distribution of the LFD histogram revealed no significant alterations in the skewness (unpaired Student's *t* test, $p = 0.30$), kurtosis (unpaired student's *t* test, $p = 0.11$), and peak frequency values (unpaired Student's *t* test, $p = 0.08$) between the two age groups

hemisphere due to ongoing edema and brain swelling. Thus, our VP technique has broad utility in normal brain vascular morphology as well as assessment in an extensive range of brain injury models.

We previously performed classical and fractal analysis to assess acute changes in the cortical vessels of adult rats after a moderate CCI and found a brain-wide reduction in vessel length, junctions, and complexity 24 h after injury [20]. Furthermore, we performed classical analysis to assess subacute changes in the cortical vessels in adult mice after a moderate CCI and found an increase in vessel density in the brain along with an increase in vessel density, length, and junctions in the peri-lesional tissue at 7 days after injury [9]. Thus, the classical and fractal analyses provide a comprehensive assessment of the cerebrovasculature in the injured brain.

Potential Applications of Vessel Painting Procedure

Further applications of the VP procedure could involve studies with magnetic resonance imaging, which would provide a unique opportunity to correlate the vascular features with neuroimaging findings. We recently demonstrated proof of

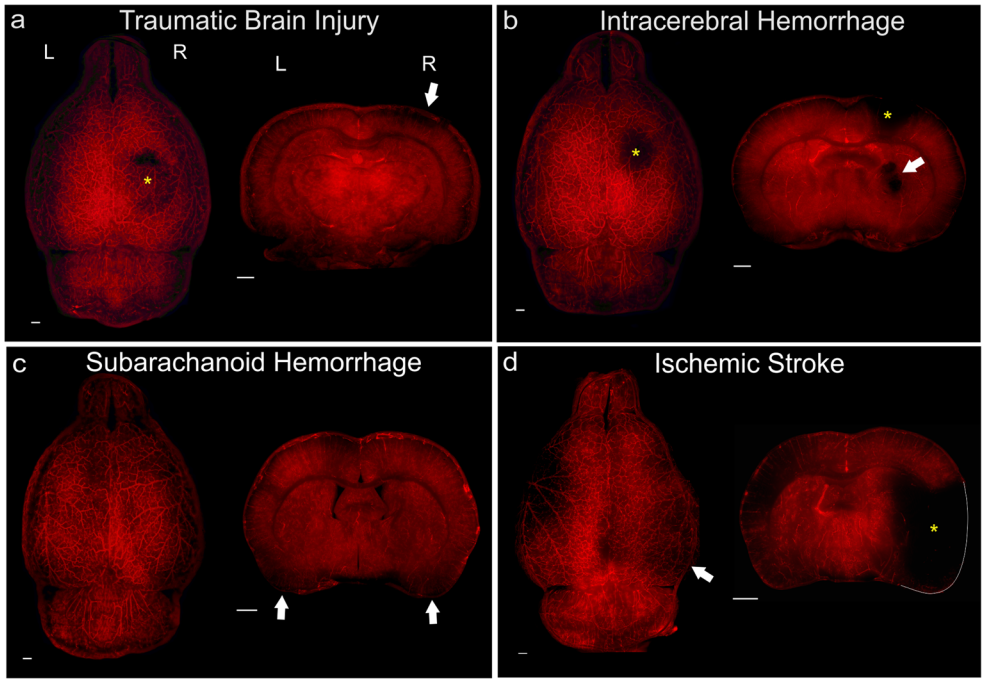

Fig. 6 Vessel painting applied to different acquired injury models. All injury models were vessel painted 24 h after injury induction. **a** Traumatic brain injury reveals a loss of cerebral vessels in the axial views on the right hemisphere (asterisk) following a controlled cortical impact model (CCI). The CCI-induced injury extends about 0.5 mm from the cortical surface (arrows) as observed in the coronal view. Right hemisphere (R) and left hemisphere (L). **b** Intracerebral hemorrhage induced by collagenase injection into the striatum reveals an injury site on the axial view (asterisk). In the coronal sections, there is a clear loss of vessels in the right striatal region (arrow). The needle track also results in a secondary loss of vessels in the cortex (yellow asterisk). **c** Subarachnoid hemorrhage model based on puncture of the middle cerebral artery (MCA) illustrates the loss of vascular complexity in the axial images, likely due to edematous brain swelling. There is loss of vascular structures at the base of the brain as can be seen in the coronal images (arrows). There is no overt injury site as the MCA puncture is at the base of the brain. **d** MCA occlusion model of stroke demonstrates a clear loss of perfusion in the right hemisphere on the axial image (solid arrows) with expansion of the right hemisphere due to edema formation. The coronal image clearly illustrates the loss of the vascular network in the region supplied by the MCA (asterisk). Scale bar = 1 mm

principle [20], where we performed correlations between individual fractal properties (skewness, kurtosis, local fractal dimensions, and peak value frequency) with total hemorrhage and edema volume from ex vivo T2-weighted imaging following moderate TBI. Combining perfusion-weighted imaging and VP could provide valuable insight into hemodynamic and cerebrovascular changes in the ischemic penumbra following MCAO. Another potential application could be combining VP with tissue-clearing solutions which would allow for imaging at depths of several millimeters along with large-scale reconstruction of the vessel structures at high resolution. The success of this method is dependent on utilizing a clearing solution devoid of organic solvents and detergents as these reagents will cause removal of the DiI from the lipid membranes of the vessels. Sca*l*eSQ, a detergent-free formulation of Sca*l*eS, could potentially be used for this purpose [38]. FocusClear has also been successfully used to clear thick brain sections following vessel painting [8]. Lastly, although we focus our investigation on the brain, the entire rodent circulatory system is exposed to DiI solution. Thus, other organs such as retinal vasculature may be stained and could be examined using our technique. It should also be noted that lipophilic tracers in the carbocyanine family are available in other colors, for example DiO is a green fluorescent marker, and are thus potentially compatible with transgenic and other types of reporter mice [21].

The VP technique we describe here produces detailed images of the cerebral vessels, but these images are restricted to depths of approximately 50 μm [39]. Several methods are available to transform the intact brain into transparent form. While these show promise in studying the cerebral vasculature, no single method provides a comprehensive view of how cerebral vessels respond to injury. One such method utilizes Tie-2/red fluorescent protein (RFP) mice and CLARITY, which allowed for imaging of cerebral vessels up to 3.2 mm into the brain [40]. However, RFP expression is controlled by an endothelial-specific promoter, and RFP expression may change under different conditions, especially in cases of brain injury and disease. The authors of this same study demonstrated that lectin and anti-claudin-5 antibody can penetrate into the CLARITY-treated brain slices of wild-type C57BL/6 mice resulting in labeling of cerebral vessels up to 900 μm [40]. However, fluorescent antibodies can lead to heterogeneous staining of vessels and nonspecific staining of nonvascular

cells. Additionally, this method has been shown to cause expansion of the brain tissue which may affect the accuracy of the quantitative analysis. Another method involves transcardial perfusion with Texas Red-labeled lectin followed by Sca*l*eA2, which leads to visualization of cerebral vessels in the hippocampus [41]. Sca*l*eA2-treated samples are often brittle, and the clearing method can potentially compromise tissue structures. This method also results in brain tissue expansion. Unlike these techniques, our VP technique uniformly stains blood vessels in different rodent strains, ages, and pathological conditions. The DiI molecules are able to laterally diffuse within the lipid membranes of the endothelial cells providing uniform staining of the vessel lumen and no staining of non-vascular cells. Thus, vessel-painted brains can be routinely used for various applications with minimal effects on the labeled vessels. Additionally, there was no overt change in the size of brain tissue using our technique.

In summary, we have developed a newly developed protocol to stain, visualize, and analyze the cerebral vasculature in the rodent brain. Among the many approaches for vessel labeling of the brain vasculature, our VP technique provides a simple, more efficient alternative that gives bright red fluorescence and exquisite resolution of the pial, penetrating, and parenchymal vessels including microvessels. Thus, the VP technique we describe will be valuable for the high-resolution imaging of the cerebral vessels in intact or injured brain. We also introduced two simple analysis approaches to assess vessel features. The classical and fractal analyses offer extensive quantitative data on vessel morphology and complexity, which have been lacking in the scientific community. Thus, these analysis techniques are critical for assessing the structural and quantitative features in the cerebral vasculature.

Acknowledgements We would like to thank Monica Romero for her assistance with the confocal imaging which was performed in the LLUSM Advanced Imaging and Microscopy Core with support of NSF Grant MRI-DBI 0923559 and the Loma Linda University School of Medicine.

Author Contributions AS, AJ, KW, MH, and AO contributed to the conception and design of the study. AS, AJ, KW, and MH acquired and analyzed the data. AS, AJ, and AO drafted a significant portion of the manuscript and figures. AO, JT, JZ, WP, RD, and ZV edited the final draft. All authors read and approved the final manuscript.

Funding Information This study was supported by an NIH Program Project grant from the National Institute of Neurological Disorders and Stroke (1P01NS082184, Project 3).

Compliance with Ethical Standards

Conflict of Interest The authors declare that they have no conflict of interest.

Research Involving Animals All procedures performed in studies involving animals were in accordance with the ethical standards of Loma Linda University Animal Health and Safety Committee (according to the Guide For the Care and Use of Laboratory Animals, Eighth edition) at which the studies were conducted.

Resource Sharing We will provide published data and relevant protocols upon request. Unpublished information can be made available by providing a request to the Principal Investigator by phone call or email.

References

1. Cipolla MJ. The cerebral circulation. integrated systems physiology: from molecule to function. San Rafael (CA) 2009.
2. Xing C, Arai K, Lo EH, Hommel M. Pathophysiologic cascades in ischemic stroke. Int J Stroke. 2012;7(5):378–85. https://doi.org/10.1111/j.1747-4949.2012.00839.x.
3. Taoufik E, Probert L. Ischemic neuronal damage. Curr Pharm Des. 2008;14(33):3565–73.
4. Muoio V, Persson PB, Sendeski MM. The neurovascular unit—concept review. Acta Physiol (Oxf). 2014;210(4):790–8. https://doi.org/10.1111/apha.12250.
5. Cauli B, Hamel E. Revisiting the role of neurons in neurovascular coupling. Front Neuroenerg. 2010;2:9. https://doi.org/10.3389/fnene.2010.00009.
6. Hughes S, Dashkin O, Defazio RA. Vessel painting technique for visualizing the cerebral vascular architecture of the mouse. Methods Mol Biol. 2014;1135:127–38. https://doi.org/10.1007/978-1-4939-0320-7_12.
7. Li Y, Song Y, Zhao L, Gaidosh G, Laties AM, Wen R. Direct labeling and visualization of blood vessels with lipophilic carbocyanine dye DiI. Nat Protoc. 2008;3(11):1703–8. https://doi.org/10.1038/nprot.2008.172.
8. Moy AJ, Wiersma MP, Choi B. Optical histology: a method to visualize microvasculature in thick tissue sections of mouse brain. PLoS One. 2013;8(1):e53753. https://doi.org/10.1371/journal.pone.0053753.
9. Salehi A, Jullienne A, Baghchechi M, Hamer M, Walsworth M, Donovan V et al. Up-regulation of Wnt/β-catenin expression is accompanied with vascular repair after traumatic brain injury. J Cereb Blood Flow Metab 2018;38(2):274–89. https://doi.org/10.1177/0271678X17744124.
10. Joshi VS, Reinhardt JM, Garvin MK, Abramoff MD. Automated method for identification and artery-venous classification of vessel trees in retinal vessel networks. PLoS One. 2014;9(2):e88061. https://doi.org/10.1371/journal.pone.0088061.
11. Bell RD, Winkler EA, Singh I, Sagare AP, Deane R, Wu Z, et al. Apolipoprotein E controls cerebrovascular integrity via cyclophilin A. Nature. 2012;485(7399):512–6. https://doi.org/10.1038/nature11087.
12. Zudaire E, Gambardella L, Kurcz C, Vermeren S. A computational tool for quantitative analysis of vascular networks. PLoS One. 2011;6(11):e27385. https://doi.org/10.1371/journal.pone.0027385.
13. Di Ieva A, Grizzi F, Jelinek H, Pellionisz AJ, Losa GA. Fractals in the neurosciences, part I: general principles and basic neurosciences. Neuroscientist. 2014;20(4):403–17. https://doi.org/10.1177/1073858413513927.
14. Di Ieva A, Esteban FJ, Grizzi F, Klonowski W, Martin-Landrove M. Fractals in the neurosciences, part II: clinical applications and future perspectives. Neuroscientist. 2015;21(1):30–43. https://doi.org/10.1177/1073858413513928.
15. Karperien A, Ahammer H, Jelinek HF. Quantitating the subtleties of microglial morphology with fractal analysis. Front Cell Neurosci. 2013;7:3. https://doi.org/10.3389/fncel.2013.00003.

16. Borodinsky LN, Fiszman ML. A single-cell model to study changes in neuronal fractal dimension. Methods. 2001;24(4):341–5. https://doi.org/10.1006/meth.2001.1204.
17. Caserta F, Eldred WD, Fernandez E, Hausman RE, Stanford LR, Bulderev SV, et al. Determination of fractal dimension of physiologically characterized neurons in two and three dimensions. J Neurosci Methods. 1995;56(2):133–44.
18. Gadde SG, Anegondi N, Bhanushali D, Chidambara L, Yadav NK, Khurana A, et al. Quantification of vessel density in retinal optical coherence tomography angiography images using local fractal dimension. Invest Ophthalmol Vis Sci. 2016;57(1):246–52. https://doi.org/10.1167/iovs.15-18287.
19. Di Ieva A, Grizzi F, Sherif C, Matula C, Tschabitscher M. Angioarchitectural heterogeneity in human glioblastoma multiforme: a fractal-based histopathological assessment. Microvasc Res. 2011;81(2):222–30. https://doi.org/10.1016/j.mvr.2010.12.006.
20. Obenaus A, Ng M, Orantes AM, Kinney-Lang E, Rashid F, Hamer M, et al. Traumatic brain injury results in acute rarefication of the vascular network. Sci Rep. 2017;7(1):239. https://doi.org/10.1038/s41598-017-00161-4.
21. Honig MG, Hume RI. Dil and diO: versatile fluorescent dyes for neuronal labelling and pathway tracing. Trends Neurosci. 1989;12(9):333–5. 40-1
22. Konno A, Matsumoto N, Okazaki S. Improved vessel painting with carbocyanine dye-liposome solution for visualisation of vasculature. Sci Rep. 2017;7(1):10089. https://doi.org/10.1038/s41598-017-09496-4.
23. Okyere B, Giridhar K, Hazy A, Chen M, Keimig D, Bielitz RC, et al. Endothelial-specific EphA4 negatively regulates native pial collateral formation and re-perfusion following hindlimb ischemia. PLoS One. 2016;11(7):e0159930. https://doi.org/10.1371/journal.pone.0159930.
24. Schindelin J, Arganda-Carreras I, Frise E, Kaynig V, Longair M, Pietzsch T, et al. Fiji: an open-source platform for biological-image analysis. Nat Methods. 2012;9(7):676–82. https://doi.org/10.1038/nmeth.2019.
25. Okyere B, Creasey M, Lebovitz Y, Theus MH. Temporal remodeling of pial collaterals and functional deficits in a murine model of ischemic stroke. J Neurosci Methods. 2017;293:86–96. https://doi.org/10.1016/j.jneumeth.2017.09.010.
26. Jullienne A, Salehi A, Affeldt B, Baghchechi M, Haddad E, Avitua A et al. Male and female mice exhibit divergent responses of the cortical vasculature to traumatic brain injury. J Neurotrauma. 2018. https://doi.org/10.1089/neu.2017.5547.
27. Harb R, Whiteus C, Freitas C, Grutzendler J. In vivo imaging of cerebral microvascular plasticity from birth to death. J Cereb Blood Flow Metab. 2013;33(1):146–56. https://doi.org/10.1038/jcbfm.2012.152.
28. Kienast Y, von Baumgarten L, Fuhrmann M, Klinkert WE, Goldbrunner R, Herms J, et al. Real-time imaging reveals the single steps of brain metastasis formation. Nat Med. 2010;16(1):116–22. https://doi.org/10.1038/nm.2072.
29. Fumagalli S, Ortolano F, De Simoni MG. A close look at brain dynamics: cells and vessels seen by in vivo two-photon microscopy. Prog Neurobiol. 2014;121:36–54. https://doi.org/10.1016/j.pneurobio.2014.06.005.
30. Shen Q, Huang S, Duong TQ. Ultra-high spatial resolution basal and evoked cerebral blood flow MRI of the rat brain. Brain Res. 2015;1599:126–36. https://doi.org/10.1016/j.brainres.2014.12.049.
31. Ostergaard L, Engedal TS, Aamand R, Mikkelsen R, Iversen NK, Anzabi M, et al. Capillary transit time heterogeneity and flow-metabolism coupling after traumatic brain injury. J Cereb Blood Flow Metab. 2014;34(10):1585–98. https://doi.org/10.1038/jcbfm.2014.131.
32. Sato Y, Nakajima S, Shiraga N, Atsumi H, Yoshida S, Koller T, et al. Three-dimensional multi-scale line filter for segmentation and visualization of curvilinear structures in medical images. Med Image Anal. 1998;2(2):143–68.
33. Zeller K, Vogel J, Kuschinsky W. Postnatal distribution of Glut1 glucose transporter and relative capillary density in blood-brain barrier structures and circumventricular organs during development. Brain Res Dev Brain Res. 1996;91(2):200–8.
34. Wang DB, Blocher NC, Spence ME, Rovainen CM, Woolsey TA. Development and remodeling of cerebral blood vessels and their flow in postnatal mice observed with in vivo videomicroscopy. J Cereb Blood Flow Metab. 1992;12(6):935–46. https://doi.org/10.1038/jcbfm.1992.130.
35. Krafft PR, Rolland WB, Duris K, Lekic T, Campbell A, Tang J, et al. Modeling intracerebral hemorrhage in mice: injection of autologous blood or bacterial collagenase. J Vis Exp. 2012;67:e4289. https://doi.org/10.3791/4289.
36. Suzuki H, Ayer R, Sugawara T, Chen W, Sozen T, Hasegawa Y, et al. Protective effects of recombinant osteopontin on early brain injury after subarachnoid hemorrhage in rats. Crit Care Med. 2010;38(2):612–8. https://doi.org/10.1097/CCM.0b013e3181c027ae.
37. Mu J, Ostrowski RP, Krafft PR, Tang J, Zhang JH. Serum leptin levels decrease after permanent MCAo in the rat and remain unaffected by delayed hyperbaric oxygen therapy. Med Gas Res. 2013;3(1):8. https://doi.org/10.1186/2045-9912-3-8.
38. Hama H, Hioki H, Namiki K, Hoshida T, Kurokawa H, Ishidate F, et al. ScaleS: an optical clearing palette for biological imaging. Nat Neurosci. 2015;18(10):1518–29. https://doi.org/10.1038/nn.4107.
39. Richardson DS, Lichtman JW. Clarifying tissue clearing. Cell. 2015;162(2):246–57. https://doi.org/10.1016/j.cell.2015.06.067.
40. Zhang Lin-Yuan, Lin Pan, Pan Jiaji, Ma Y, Wei Zhenyu, Jiang Lu et al. CLARITY for high-resolution imaging and quantification of vasculature in the whole mouse brain. Aging and Disease 2018;9(1). doi: 10.14336/ad.2017.0613.
41. Hama H, Kurokawa H, Kawano H, Ando R, Shimogori T, Noda H, et al. Scale: a chemical approach for fluorescence imaging and reconstruction of transparent mouse brain. Nat Neurosci. 2011;14(11):1481–8. https://doi.org/10.1038/nn.2928.